Tumor characterization in small animals using magnetic resonance-guided dynamic contrast enhanced diffuse optical tomography

Yuting Lin
Dave Thayer
Orhan Nalcioglu
Gultekin Gulsen

Tumor characterization in small animals using magnetic resonance-guided dynamic contrast enhanced diffuse optical tomography

Yuting Lin,ª Dave Thayer,ª Orhan Nalcioglu,ª,b,c and Gultekin Gulsenª,c
ªUniversity of California, Irvine, Tu and Yuen Center for Functional Onco-Imaging, Irvine, California 92697
bUniversity of California, Irvine, Department of Radiological Sciences, Irvine, California 92697
cPusan National University, Department of Cogno-Mechatronics Engineering, Pusan, Korea

Abstract. We present a magnetic resonance (MR)-guided near-infrared dynamic contrast enhanced diffuse optical tomography (DCE-DOT) system for characterization of tumors using an optical contrast agent (ICG) and a MR contrast agent [Gd-diethylenetriaminepentaacetic acid (DTPA)] in a rat model. Both ICG and Gd-DTPA are injected and monitored simultaneously using a combined MRI-DOT system, resulting in accurate co-registration between two imaging modalities. Fisher rats bearing R3230 breast tumor are imaged using this hybrid system. For the first time, enhancement kinetics of the exogenous contrast ICG is recovered from the DCE-DOT data using MR anatomical *a priori* information. As tumors grow, they undergo necrosis and the tissue transforms from viable to necrotic. The results show that the physiological changes between viable and necrotic tissue can be differentiated more accurately based on the ICG enhancement kinetics when MR anatomical information is utilized. © *2011 Society of Photo-Optical Instrumentation Engineers (SPIE)*. [DOI: 10.1117/1.3643342]

1 Introduction

Diffuse optical tomography (DOT) utilizes near-infrared (NIR) light to obtain spatially resolved tissue optical properties and can be used to probe tissue physiological properties based on endogenous contrast. For example, absorption coefficient increases in cancerous tissue due to elevated hemoglobin concentration,[1–5] while it reduces in breast cancer patients who respond to chemotherapy treatment due to anti-angiogenic processes.[6–8] Meanwhile, exogenous contrast agents such as FDA approved near-infrared optical agent Indocyanine green (ICG) can also be used for DOT to enhance lesion visualization due to the enhanced blood vessel growth in the cancer tissue.

ICG binds to plasma proteins *in vivo* and can be used to probe the tumor vascular permeability. There have been a few optical imaging studies using ICG as an exogenous contrast agent for breast cancer imaging. For instance, Cuccia et. al. used diffuse optical spectroscopy to show different ICG kinetics for different tumor stages with an animal model.[9] Intes et. al. and Ntziachristos et. al. used continuous wave breast DOT systems and showed different kinetics for cancerous and normal breast.[10, 11] Hagen et al. showed that invasive carcinomas retain an ICG fluorescence signal after being largely clear out from the body, indicating the high permeability of malignant tumors.[12] During the last couple of years, our center has developed a combined MRI-DOT small animal imaging system,[13] which provides a unique opportunity to utilize MRI *a priori* information for guided dynamic contrast enhanced (DCE)-DOT

reconstruction. In this study, Fisher rats bearing R3230 breast tumors are imaged at different stages by our combined MRI-DOT system. The results show that when MRI anatomical information is used to guide and constrain the DCE-DOT reconstruction process, recovered ICG enhancement kinetics differentiates the physiological changes between viable and necrotic tissue more accurately. To our knowledge, this is the first time magnetic resonance (MR) guidance is used in DCE-DOT analysis *in vivo*. The results confirm the importance of using structural *a priori* information in DCE-DOT reconstruction.

2 Method

An MR compatible frequency domain DOT system has previously been developed in our lab.[14, 15] The system operates at 100 MHz and 8 sources and 8 detectors are used, which yield 64 amplitude and 64 phase measurements. The temporal resolution of the system is 16 s, which is a pivotal feature for measuring ICG kinetics due to the fact that ICG reaches its peak concentration in about 1 min. For optical data analysis, a diffusion equation for light propagation modeling is utilized. A Levenberg–Marquardt nonlinear optimization algorithm is used for the reconstruction process. When structural *a priori* information from MRI is available, Laplacian-type soft *a priori* is utilized to guide and constrain DOT reconstruction.[16] All the reconstruction parameters, including the initial guess, damping factor, and stopping criteria, are kept the same for all the cases to ensure that there is no bias in the results. MRI setup consists of a 4T magnet with a custom-designed birdcage type RF coil, which is built into the DOT

Address all correspondence to: Yuting Lin, University of California, Irvine, Tu and Yuen Center For Functional Onco-Imaging, 164 Irvine Hall, Irvine, California 92697; Tel: 9498246001; E-mail: yutingl@uci.edu.
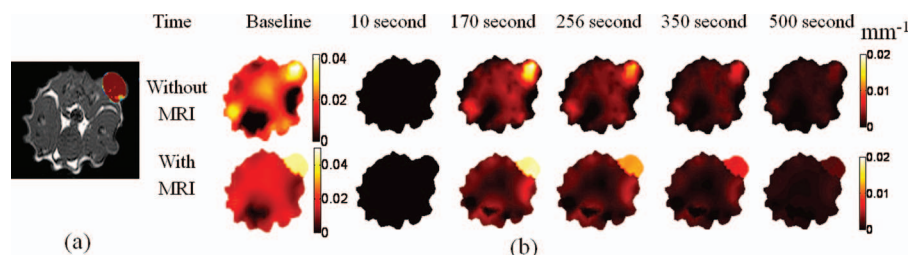
Fig. 1 (a) The T1-weighted image of a rat bearing a viable tumor. The peak Gd-DTPA enhancement on the tumor is superimposed on the anatomical image (red region). The enhancement is strong and evenly distributed within the whole tumor. (b) The ICG enhancement maps without and with MRI anatomical information are shown in the first and second row, respectively. The baseline absorption maps are shown in the first column. The next five columns of images show a time-lapse series of absorption enhancement. The tumor can be clearly seen at the peak ICG uptake (170 s) as the highest absorption area.

interface. Meanwhile, the temporal resolution of DCE-MRI is 23 s and the acquisition parameters are: 180 ms repetition time, 15 ms echo time, 90 degrees flip-angle, 120 mm field of view, 4 mm slice-thickness, and matrix size of 128×128.

All animal procedures were approved by the Institutional Animal Care and Use Committee at University of California, Irvine. Fischer rats subcutaneously implanted with R3230 adenocarcinoma breast tumor were used for this study. The cells were allowed to grow until the resulting tumor reached a size of approximately 5 mm, when the DCE-DOT studies were performed. The ICG was injected into the animals and a 785 nm laser was used to perform the DCE-DOT study, which corresponded to the peak absorption of ICG. Thirty-two frames of DOT measurements were obtained throughout each experiment. Actually, ICG was injected during the 7th frame as a single bolus together with the MR contrast agent Gd-DTPA. Hence, DCE-DOT and DCE-MRI data were acquired simultaneously, yielding an accurate co-registration between the two modalities both in space and time. The calibrated *in vivo* data was analyzed with and without MRI anatomical *a priori* information. The detailed image co-registration and mesh generation has published previously.[17]

3 Results and Discussion

The availability of DCE-MRI images permits separation of tumor tissues effectively into two different growth stages, namely, viable and necrotic.

3.1 Viable Tumor

During the early stage of tumor growth, dense blood vessels are formed due to tumor induced angiogenesis.[18] At this stage, tumor tissue is defined as viable. Due to increased blood perfusion, viable tissue displays high Gd-diethylenetriaminepentaacetic acid (DTPA) enhancement throughout the whole tumor. As an example, the T1-weighted MR image of a rat bearing a viable tumor is shown in Fig. 1(a). For this particular case, the size of the tumor is approximately 1.0 cm in diameter. The peak Gd-DTPA enhancement at the tumor region is overlaid on the anatomical image. Evidently, the enhancement is strong and evenly distributed within the tumor.

The ICG enhancement images at selected time points for the very same animal are shown in Fig. 1(b). The ICG enhancement maps are reconstructed with and without MRI anatomical

a priori information. The high ICG enhancement region correlates very well with the tumor region obtained by MRI. When MR image guidance is used, the tumor region shows more uniform distribution due to the use of *a priori* information, which tends to loosely group all the pixels within one region together, yet still allows the update of an individual pixel.
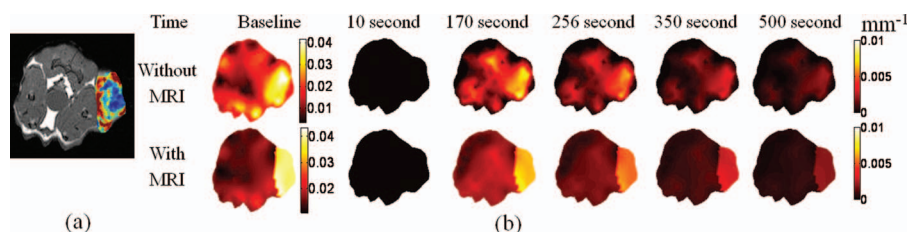
3.2 Necrotic Tumor

As tumors grow larger, the existing blood vessels undergo a regression, which in turn results in necrosis within the central part of the tumor. However, the tumor margin continues to recruit new blood vessels as a strategy to secure further growth.[19] A tumor at this stage is defined as necrotic tissue. As an example, the T1-weighted MR image of a rat bearing necrotic tumor is shown in Fig. 2(a). The size of the tumor is approximately 2.5 cm in diameter. The peak Gd-DTPA enhancement on the tumor is superimposed on the anatomical image. The tumor region shows low Gd-DTPA enhancement toward the inner aspect of the tumor, indicating the tumor has outgrown the nutrition supply and the tissue undergoes necrosis. However, the boundary still shows good blood perfusion due to the robust angiogenesis on the tumor margin.

The ICG enhancement maps are also reconstructed with and without MRI anatomical *a priori* information. Similar to the previous case, Fig. 2(b) shows ICG enhancement maps at selected time points. Again, the high ICG enhancement region correlates very well with the tumor region obtained by MRI. However, unlike MRI, DOT does not have high spatial resolution to distinguish the inner necrotic part of the tumor and the margin, which is still active. As a result, the whole tumor region displays stronger ICG enhancement compared to the surrounding tissue.

3.3 ICG Enhancement

Among all 10 animals, 5 of them were bearing viable tumors, while the others had necrotic tumors. During the analysis of ICG enhancement, the local peak absorption increase at the tumor region due to ICG was calculated for each animal. For comparison purposes, ICG peak enhancement was also calculated for a region of interest (ROI) chosen at the muscle region that was close to the tumor. The calculated values for the ROIs that corresponds to both tumor and muscle regions are presented in Table 1.

The ICG absorption change as a function of time without and with MR information is plotted in Figs. 3(a) and 3(b),

Fig. 2 (a) The T1-weighted image of a rat bearing a necrotic tumor. The peak Gd-DTPA enhancement on the tumor is overlaid on the anatomical image. The tumor region shows low Gd-DTPA enhancement (blue to green color) toward the inner aspect of the tumor, indicating the tumor has outgrown the nutrition supply and the tissue undergoes necrosis. However, the boundary (red color) still shows good blood perfusion due to the robust angiogenesis on the tumor margin. (b) The ICG enhancement maps without and with MRI anatomical information are shown in the first and second row, respectively. The baseline absorption maps are shown in the first column. The next five columns of images show a time-lapse series of absorption enhancement. The tumor can be clearly seen at the peak ICG uptake (170 s) as the highest absorption area.

respectively. Without MR guidance, there is clearly an overlap between the peak absorption increase of viable tumor and necrotic tumor. For instance, rats #7 and #10 show only 0.004 and 0.002 mm^{-1} absorption increase due to ICG for a viable tumor (highlighted in Table 1). This is even lower than rats #1, #2, #3, and #5, which all have necrotic tumors. Presumably, this may be due to the relative small size of the tumor (0.5 and 0.4 cm), resulting in an underestimated absorption increase. On the other hand, when MR anatomical information about the tumor is used to guide DOT reconstruction, the absorption increase for viable and necrotic tumors shows a significant difference, Fig. 3(b).
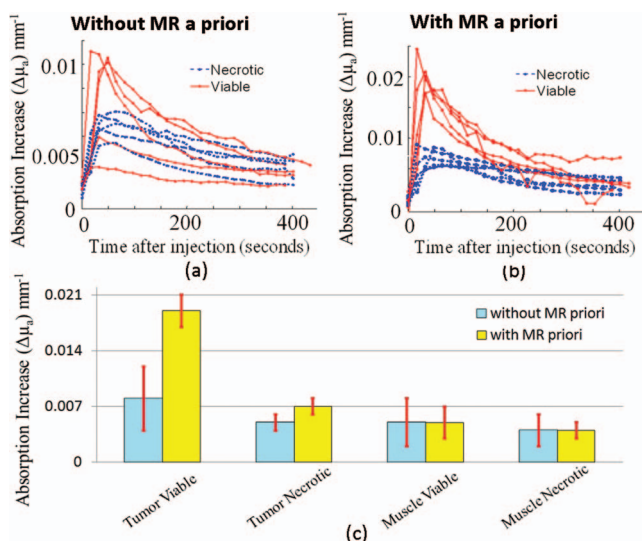
Figure 3(c) shows the mean and standard deviation for absorption increase due to ICG in the tumor region as well as surrounding muscle tissue corresponding to peak enhancement. Without the MR guidance [Fig. 3(c)], the mean $\Delta\mu_a$ is higher for the viable tumors, 0.008 ± 0.004 mm^{-1}, compared to the necrotic tumors, 0.005 ± 0.001 mm^{-1}. However, the high standard deviation values make it difficult to distinguish both stages confidently. Meanwhile, the ICG enhancement in the muscle region shows similar levels for animals with viable and necrotic tumors, 0.005 ± 0.003 and 0.004 ± 0.002 mm^{-1}, respectively, and the error bars for the two groups overlap with each other.

On the other hand, when MR *a priori* is used [Fig. 3(c)], the difference between mean $\Delta\mu_a$ for both tumor stages increases drastically: 0.019 ± 0.002 and 0.007 ± 0.001 mm^{-1} for viable and necrotic tumors, respectively. Meanwhile, the ICG enhancement in the muscle region still shows similar

Table 1 Summary of tumor stages for 10 animals. The absorption increase due to ICG ($\Delta\mu_a$) at both tumor and muscle regions for each animal are shown. The unit for $\Delta\mu_a$ is mm^{-1} and the unit for a tumor size is millimeters. Although animals #7 and #10 has viable tumors, the absorption increase due to ICG is similar to necrotic tumors (highlighted). However, when *a priori* information is utilized, $\Delta\mu_a$ in the tumor region becomes similar to other viable tumors. The mean values for both groups are also provided together with the standard deviation values.

Rat no.	Tumor stage	Tumor size	$\Delta\mu_a$ tumor wo/MR	$\Delta\mu_a$ tumor w/MR	$\Delta\mu_a$ muscle wo/MR	$\Delta\mu_a$ muscle w/MR
1	Necrotic	2.1	0.005	0.006	0.002	0.002
2	Necrotic	2.0	0.006	0.007	0.004	0.004
3	Necrotic	1.4	0.006	0.006	0.003	0.003
4	Necrotic	2.2	0.003	0.008	0.005	0.004
5	Necrotic	1.6	0.005	0.008	0.006	0.006
	Mean		*0.005 ± 0.001*	*0.007 ± 0.001*	*0.004 ± 0.002*	*0.004 ± 0.001*
6	Viable	1.0	0.010	0.018	0.002	0.004
7	Viable	0.5	0.004	0.021	0.003	0.004
8	Viable	1.5	0.011	0.017	0.007	0.004
9	Viable	1.2	0.011	0.020	0.006	0.007
10	Viable	0.4	**0.002**	**0.020**	**0.008**	**0.008**
	Mean		*0.008 ± 0.004*	*0.019 ± 0.002*	*0.005 ± 0.003*	*0.005 ± 0.002*

Fig. 3 The ICG dynamic enhancement time course curves obtained using the recovered mean absorption coefficient in the ROI without and with MRI are shown in (a) and (b), respectively. The mean and standard deviation for absorption at the peak ICG enhancement in the tumor region as well as surrounding muscle tissue without and with MRI are shown in (c). Viable and necrotic stages are indicated with solid and dashed lines, respectively.

levels for animals bearing different tumor stages (viable: 0.005 ± 0.002 mm^{-1} and necrotic: 0.0038 ± 0.001 mm^{-1}). Please note that standard deviation in the $\Delta\mu_a$ values also decreases particularly for viable tumors when MR *a priori* information is used to guide and constrain the DOT reconstruction.

4 Conclusion and Discussion

In summary, we presented spatially-resolved dynamic enhancement kinetics of ICG using a hybrid DOT-MRI system *in vivo*. The hybrid system allowed carrying out the DCE-DOT analysis using MR anatomical information. The results confirmed the performance of DCE-DOT in tumor localization. However, only when MRI *a priori* information was utilized, ICG enhancement showed a significant difference for the two tumor stages. These results confirmed that a hybrid DCE-DOT system can be an effective tool for characterization of tumor stages by providing an accurate ICG enhancement amount. As the next step, ICG kinetics will also be analyzed to provide additional information for tumor diagnosis and therapy monitoring.

References

1. R. Choe, et al., "Differentiation of benign and malignant breast tumors by in-vivo three-dimensional parallel-plate diffuse optical tomography," *J. Biomed. Opt.* **14**(2), 024020 (2009).
2. A. Cerussi, N. Shah, D. Hsiang, A. Durkin, J. Butler, and B. J. Tromberg, "In vivo absorption, scattering, and physiologic properties of 58 malignant breast tumors determined by broadband diffuse optical spectroscopy," *J. Biomed. Opt.* **11**(4), 044005 (2006).
3. Q. Fang, J. Selb, S. A. Carp, G. Boverman, E. L. Miller, D. H. Brooks, R. H. Moore, D. B. Kopans, and D. A. Boas, "Combined optical and x-ray tomosynthesis breast imaging," *Radiology* **258**(1), 89–97 (2011).
4. V. Ntziachristos and B. Chance, "Probing physiology and molecular function using optical imaging: applications to breast cancer," *Breast Cancer Res.* **3**(1), 41–46 (2001).
5. A. Yodh and B. Chance, "Spectroscopy and imaging with diffusing light," *Phys. Today* **48**, 34–40 (1995).
6. C. Zhou, et al., "Diffuse optical monitoring of blood flow and oxygenation in human breast cancer during early stages of neoadjuvant chemotherapy," *J. Biomed. Opt.* **12**(5), 051903 (2007).
7. A. Cerussi, D. Hsiang, N. Shah, R. Mehta, A. Durkin, J. Butler, and B. J. Tromberg, "Predicting response to breast cancer neoadjuvant chemotherapy using diffuse optical spectroscopy," *Proc. Natl. Acad. Sci. U.S.A.* **104**(10), 4014–4019 (2007).
8. S. Jiang, et al., "Evaluation of breast tumor response to neoadjuvant chemotherapy with tomographic diffuse optical spectroscopy: case studies of tumor region-of-interest changes1," *Radiology* **252**(2), 551–560 (2009).
9. D. J. Cuccia, F. Bevilacqua, A. J. Durkin, S. Merritt, B. J. Tromber, G. Gulsen, H. Yu, J. Wang, and O. Nalcioglu, "In vivo quantification of optical contrast agent dynamics in rat tumors by use of diffuse optical spectroscopy with magnetic resonance imaging coregistration," *Appl. Opt.* **42**(16), 2940–2950 (2003).
10. X. Intes, J. Ripoll, Y. Chen, S. Nioka, A. G. Yodh, and B. Chance, "In vivo continuous-wave optical breast imaging enhanced with Indocyanine Green," *Med. Phys.* **30**(6), 1039–1047 (2003).
11. V. Ntziachristos, A. G. Yodh, M. Schnall, and B. Chance, "Concurrent MRI and diffuse optical tomography of breast after indocyanine green enhancement," *Proc. Natl. Acad. Sci. U.S.A.* **97**(6), 2767–2772 (2000).
12. A. Hagen, D. Grosenick, R. Macdonald, H. Rinneberg, S. Burock, P. Warnick, A. Poellinger, and P. M. Schlag, "Late-fluorescence mammography assesses tumor capillary permeability and differentiates malignant from benign lesions," *Opt. Express* **17**(19), 17016–17033 (2009).
13. G. Gulsen, B. Xiong, O. Birgul, and O. Nalcioglu, "Design and implementation of a multifrequency near-infrared diffuse optical tomography system," *J. Biomed. Opt.* **11**(1), 014020 (2006).
14. M. B. Unlu, Y. Lin, and G. Gulsen, "Dynamic contrast-enhanced diffuse optical tomography (DCE-DOT): experimental validation with a dynamic phantom," *Phys. Med. Biol.*, **54**(21), 6739–6755 (2009).
15. G. Gulsen, O. Birgul, M. B. Unlu, R. Shafiiha, and O. Nalcioglu, "Combined diffuse optical tomography (DOT) and MRI system for cancer imaging in small animals," *Technol. Cancer Res. Treat* **5**(4), 351–363 (2006).
16. P. K. Yalavarthy, B. W. Pogue, H. Dehghani, C. M. Carpenter, S. Jiang, and K. D. Paulsen, "Structural information within regularization matrices improves near infrared diffuse optical tomography," *Opt. Express* **15**(13), 8043–8058 (2007).
17. M. Ghijsen, Y. Lin, M. Hsing, O. Nalcioglu, and G. Gulsen, "Optimal analysis method for dynamic contrast-enhanced diffuse optical tomography," *It. J. Biomed. Imaging* **2011** (2011).
18. P. Carmeliet and R. K. Jain, "Angiogenesis in cancer and other diseases," *Nature* **407**(6801), 249–257 (2000).
19. J. W. S. Holash and G. D. Yancopoulos, "New model of tumor angiogenesis: dynamic balance between vessel regression and growth mediated by angiopoietins and VEGF," *Oncogene* **18**(38), 5356–5362 (1999).